X-ray resonant Raman cross section and yield in nickel

S. Manninen and P. Suortti
Department of Physics, University of Helsinki, Siltavuorenpenger 20D, SF-00170 Helsinki 17, Finland

M. J. Cooper
Department of Physics, University of Warwick, Coventry CV4 7AL, England, United Kingdom

J. Chomilier and G. Loupias*
Laboratoire de Minéralogie-Cristallographie, Université Pierre et Marie Curie (Paris VI) et Université de Paris VII, Tour 16, 4 place Jussieu, 75252 Paris Cédex 05, France

(Received 8 July 1986)

The resonant enhancement of Raman scattering from nickel was studied with monochromatic synchrotron radiation at incident energies just below the K absorption edge. The intensities of the KL and KM contributions were recorded through the transition from resonant Raman scattering (RRS) to fluorescence and the yield was determined. The scattering cross section immediately below and above the fluorescence threshold reflected the density of states and followed the predictions of simple RRS calculations.

I. INTRODUCTION

KL or KM resonant Raman scattering (RRS) occurs when the energy of the incident x-ray photon is just below the K absorption threshold of the target. It proceeds by a virtual K-shell hole in the intermediate state to a final state in which there is an L-shell or M-shell hole, an electron in the continuum, and an emitted photon. Higher shells may be involved in heavier materials (e.g., KN-RRS). The process is shown schematically in Fig. 1. As the photon energy, $\hbar\omega_1$, approaches the threshold K-shell binding energy $\hbar\Omega_{1s}$, the scattered intensity increases approximately as $(\Omega_{1s}-\omega_1)^{-1}$. The spectrum is continuous because the photon and the electron share the available energy, $\hbar\omega_1-\hbar\omega_{np_j}$ where np_j denotes the final hole state, e.g., $2p_{1/2}$ or $2p_{3/2}$ for KL-RRS.

Although the resonant Raman effect was first observed in x-ray scattering more than one decade ago[1] there have been relatively few quantitive studies to date. Its measurement is important because it contributes strongly to the photoelectric absorption coefficient near the threshold. It is also likely that high-resolution studies will reveal a structure similar to extended-x-ray-absorption fine structure (EXAFS) phenomena due to the backscattering of the ejected electrons. Correlation effects are also potentially important in this two-electron process.

A. Background theory

In terms of semiclassical radiation theory the scattering occurs through the $\bar{p}\cdot\bar{A}$ term in second order, not the A^2 term which accounts for elastic, Compton, and normal Raman scattering.[2] The effect was predicted by Gavrila and Tugulea[3] and the underlying theory has been reviewed recently by Åberg and Tulkki.[4] The differential cross section per unit frequency for the K-resonance scattering by np_j electrons is

$$\frac{d\sigma(\omega_1)}{d\omega_2}=2\pi r_0^2\int_0^\infty\left[\frac{\omega_2}{\omega_1}\right]\frac{(\Omega_{1s}-\Omega_{np_j})g_{np_j,1s}(\Omega_{1s}+\omega)(dg_{1s}/d\omega)}{(\Omega_{1s}+\omega-\omega_1)^2+\Gamma_{1s}^2/4\hbar^2}\delta(\omega_1-\Omega_{np_j}-\omega-\omega_2)d\omega\ . \tag{1}$$

Here $\hbar\omega_2$ is the energy of the scattered photon, $\hbar\omega$ the kinetic energy of the ejected electron, and Γ_{1s} the width of the $1s$ level. The oscillator strength of the transition between the $1s^{-1}$ and $np_j{}^{-1}$ hole states is given by $g_{np_j,1s}$ and the oscillator density $dg_{1s}/d\omega$ is proportional to the density of states. The final-state lifetimes can be included in Eq. (1) by replacing the δ function by a normalized Lorentzian of width Γ_{np_j}.

If the final-state effects are ignored, and the condition $\omega_2+\omega=\omega_1-\Omega_{np_j}$ is used, the average differential cross section per unit frequency and solid angle for the scattering by $2p_j$ electrons ($j=\frac{1}{2},\frac{3}{2}$) is

$$\frac{d^2\sigma}{d\omega_2 d\Omega}=\frac{r_0^2}{2}\frac{\omega_2}{\omega_1}\times\frac{(\Omega_{1s}-\Omega_{2p_j})g_{2p_j,1s}(\Omega_{1s}+\omega)}{(\Omega_{1s}-\Omega_{2p_j}-\omega_2)^2+\Gamma_{1s}^2/4\hbar^2}\left[\frac{dg_{1s}}{d\omega}\right]_{\Omega_{1s}+\omega}\ . \tag{2}$$

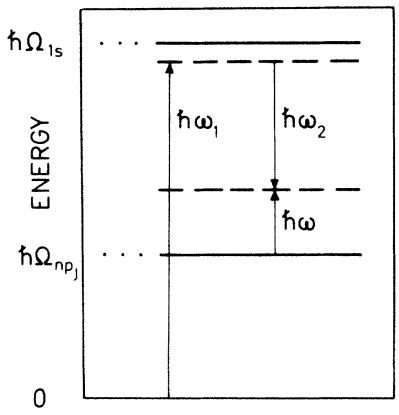

FIG. 1. Schematic energy digram of KL-resonant Raman scattering. The energy of the incident photon, $\hbar\omega_1$, is less than the threshold energy for photoelectric absorption $\hbar\Omega_{1s}$. The available energy, $\hbar\omega_1-\hbar\omega_{2p}$, is shared between the outgoing photon ($\hbar\omega_2$) and the ejected electron ($\hbar\omega$).

It is seen that above the threshold, where ω_2 has a Lorentzian distribution centered at $\Omega_{1s}-\Omega_{2p_j}$, the integrated cross section $d\sigma/d\Omega$ follows the oscillator density (or the density of states) as a function of the energy of the ejected electron, $\hbar\omega$, and $d\sigma/d\Omega$ is convoluted by this Lorentzian of width Γ_{1s}. On the other hand, sufficiently far below the threshold ($dg_{1s}/d\omega$) can be replaced in the integration by the value that corresponds to the average energy of the ejected electron, $\hbar\bar{\omega}$. The leading term is[5]

$$\left[\frac{d\sigma}{d\Omega}\right]_{KL} \approx \frac{(\Omega_{1s}+\bar{\omega})}{4\pi^2\omega_1}\sigma_{1s}(\Omega_{1s}+\bar{\omega})\tan^{-1}\left[\frac{\Gamma_{1s}/2}{\Delta E}\right], \quad (3)$$

where $\sigma_{1s}(\Omega_{1s}+\bar{\omega})$ is the KL contribution to the photoelectric absorption coefficient and $\Delta E=\hbar(\Omega_{1s}-\omega_1)$. If the density of states were a simple step function, the cross section at $\Delta E=0$ would be $\frac{1}{2}$ of that for full fluorescence, i.e.,

$$4\pi\left[\frac{d\sigma}{d\Omega}\right]_{KL}=\tfrac{1}{2}\sigma_{1s}(\Omega_{1s}) . \quad (4)$$

When $\Delta E \gg \Gamma_{1s}$ the resonant cross section reduces to a simple hyperbolic expression, and

$$\left[\frac{d\sigma}{d\Omega}\right]_{KL} \approx \frac{\Gamma_{1s}}{8\pi^2\Delta E}\frac{(\Omega_{1s}+\bar{\omega})}{\omega_1}\sigma_{1s}(\Omega_{1s}+\bar{\omega}) . \quad (5)$$

The cross section is independent of the scattering angle and the polarization state of the incident beam in this nonrelativistic approximation. Tulkki and Åberg[6] have predicted higher-order anisotropic interference effects in the cross section but these appear to be beyond the accuracy of present measurements.[7]

B. Proposed investigation

Most x-ray studies to date[5,8,9] have concentrated on the more intense KL transition and have used low-energy (<10 keV) synchrotron radiation or characteristic x rays. Recent measurements at higher energies have rendered the splitting between $1s$, $2p_{1/2}$ and $1s$, $2p_{3/2}$ resonant lines visible with the modest resolution of a solid-state detector. The KM line shape in ytterbium was studied by Manninen *et al.*[10] with 60 keV gamma rays and the KM resonance was observed in neodymium with 43 keV synchrotron radiation by Schaupp *et al.*[11]

Eisenberger *et al.*[8] measured the intensity variation of the KL-RRS in copper through the threshold, and Czerwinski *et al.*[7] obtained the KL and KM cross sections on an absolute scale to within 40 eV of the threshold in xenon. In the former work the intensity scale was not established and in neither experiment was the region just below the threshold studied in detail. The present studies were directed to the measurement of the resonant Raman yield—that is the ratio of x-ray emission in the KL and KM scattering processes to absorption—as well as the absolute cross section through the transition from RRS to x-ray fluorescence. Previous measurements[6] of the yield have been restricted to characteristic x-ray energies but synchrotron radiation is the obvious source for such a study not only because of its tuneability and brightness but also of its polarization. The latter is important because it means that elastic and Compton scattering can be suppressed by choosing a scattering angle of 90° in the machine's orbital plane.

II. EXPERIMENT

A. The resonance Raman spectra

Radiation from the Laboratorie d'Utilisation du Rayonnement Electromagnétique (LURE)-DCI storage ring, operating at an electron energy of 1.72 GeV, was collimated down to a cross section 0.50 mm high by 8 mm wide and monochromated by the (220) reflections from a pair of symmetrically-cut silicon crystals. The resolution of the monochromator was 1 eV at 8 keV and it delivered a flux of the order of 10^7 photons/sec onto the nickel samples. The experimental arrangement is shown in Fig. 2; the flux of the incident beam was monitored by an ionization chamber and the scattered radiation detected by an intrinsic silicon detector which had a resolution (FWHM) of 170 eV at 8 keV. Incident energies in the range 8200–8350 eV (the Ni K-absorption edge is centered at 8333 eV) were selected and the KL- and KM-RRS spectra

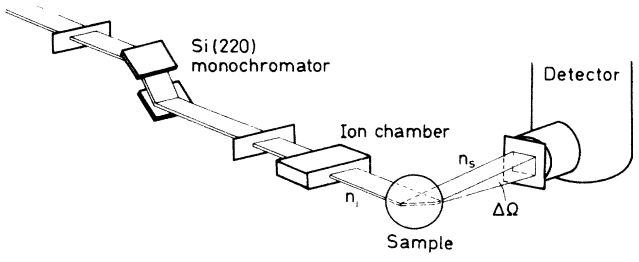

FIG. 2. Schematic diagram of the experimental arrangement.

recorded. The solid-state detector essentially had constant efficiency (100%) across this range but the absorption of radiation by the ion chamber gas has an $(\hbar\omega_1)^{-3}$ variation while the number of ion pairs produced is proportional to $\hbar\omega_1$. Thus the intensities were scaled as the production of the ionization current I and $(\hbar\omega_1)^2$. It was not necessary to determine the intensity of the incident beam on an absolute scale since that scale is inferred from the known fluorescence yield (see Sec. III below).

Measurements were concentrated in the narrow energy range around the edge (8320—8345 eV) where the resonant intensities are highest, the energy being changed in 1 eV steps between each run. Just below the absorption threshold 250 sec were sufficient to accumulate approximately 10^5 counts under the KL and KM lines, progressively longer times being necessary further away from the threshold. In all, the following three samples were studied: (i) a [100] single-crystal slice, (ii) a powder disc, and (iii) a 25 μm polycrystalline foil; (i) and (ii) were "thick" samples and were measured in symmetric reflection whereas the third was oriented for symmetric transmission. Three typical spectra are reproduced for illustration in Fig. 3. Two features are readily evident; firstly the rapid increase of intensity as $\hbar\omega_1 \rightarrow \hbar\Omega_K$ and secondly the shift of the RRS peak towards the limiting characteristic K-fluorescence emission energy at the threshold. Near to this threshold the resonant Raman lines are narrower than the detector response function and their shape is masked, but in Fig. 3(a), at the lowest energy shown, the asymmetry that originates from the Lorentzian tail is clearly seen.

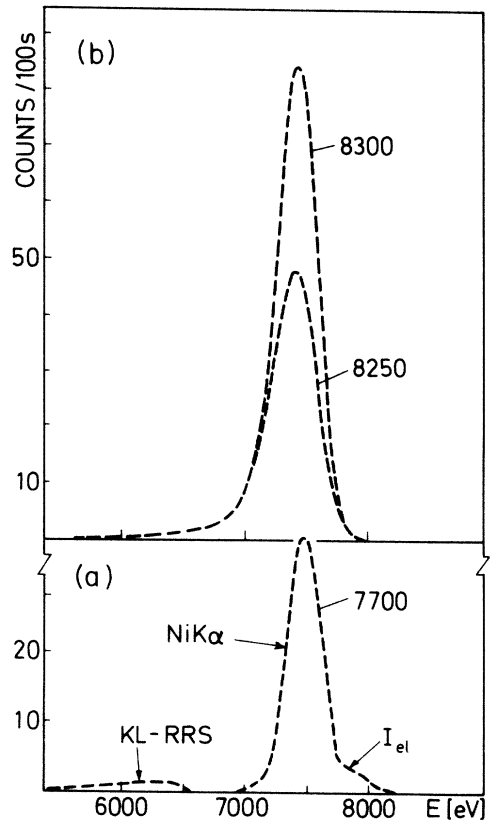

FIG. 3. KL-RRS spectra at three different incident energies (a) $\hbar\omega_1 = 7700$ eV, Ni $K\alpha$ and elastic scattering contributions are also seen separately, (b) $\hbar\omega_1 = 8250$ eV, 8300 eV.

The energy scale indicated by the monochromator calibration was checked from time to time by measuring the nickel absorption edge in an EXAFS measurement using a 6 μm foil in front of the ionization chamber. If the density of final states were a constant, Eq. (4) could be easily applied to determine the true energy scale. In the case of nickel, there are several band-structure calculations and the density of empty p states above the Fermi level is well known[12] (in the dipole approximation only transitions from np_j to $1s$ states are allowed). The energy scale can therefore be determined by fitting the measured absorption coefficient $\mu_k(E)$ with the theoretical curve. This was checked independently using Eq. (3) and the experimental values (after contributions due to absorption from higher shells were subtracted) sufficiently far below the threshold energy. It turned out that the latter method was very sensitive, giving the accuracy better than 0.5 eV to the position of the threshold energy.

The integrated intensities of the lines depicted in Fig. 3 cannot be used directly to calculate the KM:KL ratio or the resonant Raman yield because they may include other spurious scattering contribution such as elastic scattering, or Ni fluorescence excited by the first harmonic of the monochromator. These contributions are not separately resolved by the solid-state detector.

B. Elastic scattering

Some contribution through the A^2 term is possible, even if the ideal scattering angle of 90° in the orbital plane has been selected, for two reasons. Firstly, the finite source size and vertical collimation admits approximately 3% of the perpendicular polarization to the monochromator although after two reflections it is less than 2% and, secondly, the range of scattering angles subtended by the detector allows some scattering of the parallel polarization.

In a preliminary experiment with a polycrystalline foil sample a measurable contribution from the Ni(311) Bragg reflection was found at $\hbar\omega_1 = 8255$ eV when $2\theta_{\text{Bragg}} = 90°$. At that energy it overlapped the KM-RRS peak, enhancing the apparent intensity by approximately 30%. Although this parasitic contribution can be completely avoided when the oriented single-crystal sample is used, $2\theta_{\text{Bragg}} = 87°$ was selected because the range of interest was then between the (220) and (311) Bragg peaks. The foil and powder samples also could then be safely studied.

With diffraction eliminated and Compton scattering negligible at these energies only the weak elastic thermal diffuse scattering (TDS) remains. The resolution of the solid-state detector is not adequate to separate TDS completely from the KM line. Fortunately the energy variation of TDS in nickel at x-ray energies is well known;[13] therefore it was measured at lower energies ($\hbar\omega_1 = 7000$, 7400, and 7700 eV were chosen) where there is no RRS intensity and the result extrapolated to the range of interest.

At 10 eV below the fluorescence threshold TDS contributes a few percent to the measured KM intensity.

C. X-ray fluorescence

It is evident from Fig. 3 that the resonant Raman lines, as recorded by a solid-state detector, will overlap any fluorescence emissions excited in the target by monochromator harmonics. Accordingly the fluorescent intensities were determined at several energies in the range 7000 (where RRS is negligible) to 8000 eV (where the contributions are separable). These intensities were then extrapolated to the measurement range, 8200–8350 eV, taking into account the energy variation of sample absorption and the source flux at the energy $\hbar\omega_1$. The contribution to each RRS peak was a few percent at 10 eV below the threshold. In the case of fluorescence as well as TDS small errors in their estimation will have a negligible effect upon the corrected intensities close to the threshold.

III. DETERMINATION OF THE RESONANT RAMAN YIELD AND CROSS SECTION

The hole in the K shell can be filled without the emission of a photon through the competing Auger process. If $(d\sigma/d\Omega)_K$ is the K-shell photoelectric absorption cross section, then the resonant Raman yield ω_{RRS} is simply the ratio, vis.,

$$\omega_{\mathrm{RRS}}=\left[\frac{d\sigma}{d\Omega}\right]_{\mathrm{RRS}}\Big/\left[\frac{d\sigma}{d\Omega}\right]_K , \tag{6}$$

or $\omega_{\mathrm{RRS}}=\sigma_{\mathrm{RRS}}/\sigma_K$, if both processes are isotropic.

The yield can be expressed in terms of the incident, n_i, and scattered, n_s, photon fluxes as follows for the symmetric scattering geometries shown in Fig. 2. For a thick sample in reflection

$$\frac{n_s}{n_i}=\frac{\Delta\Omega\omega_{\mathrm{RRS}}}{4\pi}\,\frac{\mu_K(\omega_1)}{\mu(\omega_1)+\mu(\omega_2)} , \tag{7}$$

where $\mu_K(\omega_1)$ is the K-shell absorption coefficient and $\mu(\omega_1)$ and $\mu(\omega_2)$ are the total attenuation coefficients for the incoming and outgoing beams. For transmission through a sample of thickness T the analogous expression is

$$\frac{n_s}{n_i}=\frac{\Delta\Omega}{4\pi}\,\omega_{\mathrm{RRS}}\mu_K(\omega_1) \times\frac{\exp[-\mu(\omega_2)T/\cos\theta]-\exp[-\mu(\omega_1)T/\cos\theta]}{\mu(\omega_1)+\mu(\omega_2)} . \tag{8}$$

Thus the yield can be calculated directly with an accuracy dependent upon the determination of the incident flux and the uncertainty in the absorption coefficients. In this analysis the former of these problems was circumvented by measuring the fluorescence intensity at several energies just above the threshold and using the fact that the fluorescence yield, ω_K, is a well-determined quantity. The measured value 0.432 ± 0.006 (Ref. 4) agrees well with a calculated value of 0.433 based upon a Hartree-Fock-Slater (HFS) calculation.[14] The assumption of a value for n_F essentially determines the quantity $n_i\Delta\Omega$ in Eqs. (7) and (8), leaving only the attenuation coefficients to be ascertained. These were deduced from an initial measurement of the intensity transmitted through a 6 μm nickel foil as the monochromator was scanned (this measurement was also used to confirm the energy scale from the location of the absorption edge). The attenuation coefficient was measured between 8100 and 8400 eV using an ionization chamber. The logarithm of the count rate was displayed so that the difference between the readings with

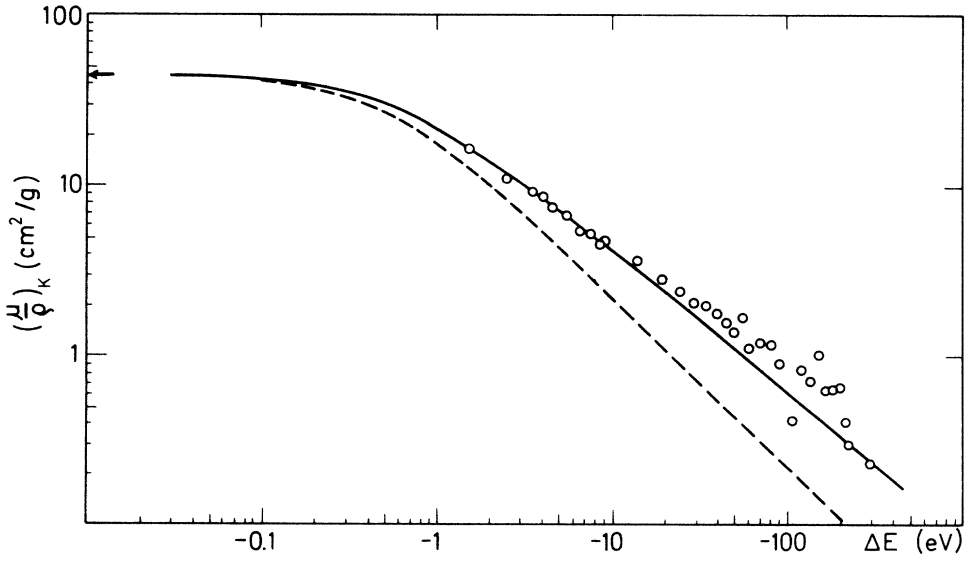

FIG. 4. K-shell contribution to the mass-absorption coefficient of Ni. The experimental values (open circles) are obtained from the measured attenuation coefficient by subtracting the higher-shell contribution using extrapolation. Theoretical values calculated from the density of $2p$ states (Ref. 12) are given by the solid line, and the dashed line indicates the corresponding values for a constant density of final states.

and without the absorber was proportional to the absorption coefficient. The values given in the *International Tables for X-ray Crystallography* were used as references.[15] Above the edge, $\mu/\rho = 344$ cm^2 g^{-1} at 8360 eV, and below the edge μ/ρ was set to be 49.06 cm^2 g^{-1} at 8041 eV by estimating the RRS contribution at 0.23 cm^2 g^{-1} from Eq. (5). The results are not sensitive to the choices of the reference values as long as these values are compatible.

The attenuation coefficient below the K-absorption edge is primarily due to photoabsorption in L and higher shells. This contribution must be subtracted from the measured total absorption coefficient before the K-shell cross section can be analyzed. The subtraction is based on an extrapolation from the same tabulated values that are used in determination of the scale of the measured absorption coefficient. It is obvious that these values do not include the effects of the resonant scattering below the K edge, but follow a simple power law. The values of μ/ρ at 8041 eV (CuK$\bar{\alpha}$) and 8265 eV (NiKβ_1) were used as references, and the resulting expression for the higher-shell contribution is

$$(\mu/\rho)_{L,M} = 48.83(8041 \text{ eV}/E)^{2.78} \text{ cm}^2 \text{ g}^{-1} .$$

The higher-shell contribution, which includes also the slowly varying scattering cross sections, was subtracted from $(\mu/\rho)_{\text{exp}}$ to leave $\mu_K(\omega_1)/\rho$, the K-shell contribution. The result is shown in Fig. 4. Below the absorption edge, the values are larger than those due to the step $\Delta(\mu_K/\rho) = 90$ cm^2 g^{-1} at $E = 0$, which is inferred from the calculated density of p states,[12] but follow closely the curve after the effect of the density of p states above the edge is taken into account (this was done using numerical integration based on data given in Ref. 12). A small adjustment of the energy scale was inferred from a comparison of measured and calculated values and the correction made. The yield and the KL:KM ratio were then calculated and the results were then transformed into the scattering cross section using Eq. (6). These experimentally-deduced cross sections are presented in Table I.

TABLE I. The table lists the K-shell radiative yield, ω_{RRS} below the absorption threshold, ω_K above it, the ratio of KM scattering to KL scattering, the K-shell contribution to the total absorption, $\mu_K(\omega_1)$, and the RRS cross section per unit solid angle, $(d\sigma/d\Omega)_K$. Results are based on three different Ni samples, single crystal (SC), powder sample (PS) and foil (F). The energy scale ΔE is relative to the K-shell absorption threshold (8333 eV) and the values of ω_{RRS} (ω_K) are very sensitive to errors in the establishment of that scale in the range $-8.5 \leq \Delta E \leq 2.5$ eV. The fluorescence yield for the single-crystal measurement was normalized to the reference value of 0.432 at $\Delta E = +18.5$ eV and the values for powder sample and foil were normalized to the single-crystal value at $\Delta E = +11.5$ eV. The scattering cross section, $(d\sigma/d\Omega)_K$, is calculated from Eq. (6) and quoted in units of the Thompson cross section.

	$\omega_{\text{RRS}}, \omega_K$			KM:KL				
ΔE	SC	PS	F	SC	PS	F	$\mu_K(\omega_1)$ (cm^{-1})	$(d\sigma/d\Omega)_K$ (e.u.)
−133.5		0.250	0.326		0.225	0.256	5.9	18.6
−83.5		0.320			0.163		8.5	29.8
−58.5		0.339	0.321		0.169	0.200	11.1	40.2
−43.5		0.378			0.152		13.4	55.5
−33.5		0.405	0.389		0.144	0.169	16.5	71.8
−23.5	0.381	0.418		0.152	0.151		21.4	93.8
−18.5		0.416	0.422		0.149	0.158	25.8	118
−13.5		0.452	0.433		0.160	0.158	31.2	151
−8.5		0.467	0.499		0.154	0.152	42.8	227
−3.5	0.482	0.482		0.160	0.156		81.7	431
−1.5	0.503			0.154			147	812
+0.5	0.446			0.158			494	2419
+1.5		0.466	0.433		0.157	0.165	696	3432
+2.5	0.472			0.157			854	4423
+3.5	0.458			0.162			951	4776
+4.5	0.444			0.157			1023	4985
+5.5	0.440			0.159			1082	5220
+6.5	0.439	0.446	0.439	0.157	0.162	0.162	1176	5694
+7.5	0.439			0.152			1264	6085
+8.5	0.436			0.161			1360	6504
+9.5	0.432			0.158			1471	6970
+10.5	0.434			0.161			1591	7573
+11.5	0.439	0.439	0.439	0.160	0.158	0.164	1749	8422
+12.5	0.432			0.159			1931	9149
+13.5	0.428			0.160			2156	10 122
+14.5	0.433			0.160			2335	11 086
+15.5	0.431			0.157			2471	11 680
+16.5	0.430			0.157			2542	11 987
+18.5	0.432			0.159			2557	12 113

IV. DISCUSSION

The radiative yield of a scattering process is the ratio of the emitted radiation to the absorbed radiation when appropriate corrections for self-absorption and other geometry-dependent factors are made. In the present case there are one photon and one electron in the radiative channel and two electrons in the Auger channel. It is seen from Table I that the radiative yield first increases slightly when the incident energy decreases below the threshold energy, but from about $\Delta E = -15$ eV the yield falls steadily with ΔE. Unfortunately, the uncertainties of the measurement are too large to allow firm conclusions. A small drift in the energy scale (about 0.2 eV) is enough to cause the apparent increase of ω_K between $+5$ and -10 eV, and $(\mu/\rho)_K$ depends critically on the correctness of the subtraction of the higher shells contribution from the measured (μ/ρ). For instance, if the values estimated from the density of the $2p$ states are used for $(\mu/\rho)_K$, the RRS yield becomes almost equal to that of fluorescence.

There are no theoretical calculations of ω_{RRS}, and no obvious reason why the value for fluorescence, ω_K, should prevail far below the K edge. The need of reliable experimental data is therefore evident. The quality of the present data could be improved in various ways. Radiation from a multipole wiggler is linearly polarized also outside the orbit plane, and the intensity is much larger than that from a bending magnet source. The use of a Si(311) monochromator would make the harmonic contamination almost negligible and also improve the energy resolution. All these features combined would make possible fast collection of resonant scattering intensities with minimum interference of parasitic scattering. The K-shell absorption cross section can be separated from the total attenuation coefficient, if the measurements cover a sufficiently large energy range below the K edge. Theoretical values of $(\mu/\rho)_K$ can be calculated from Eqs. (1) or (2), if the density of $2p$ states and the transition probabilities are known. Typically, the calculated $(\mu/\rho)_K$ has too much structure above the threshold, and also the values far below the edge may be only approximately correct.

The ratio of the KM scattering to the KL scattering is primarily determined by the ratio of the respective oscillator strengths, as seen from Eq. (1). These are constant, and this is also seen from the results of Table I. The upward deviations at small energies are presumably due to an incomplete removal of the elastic scattering contribution.

These measurements are the first to chart the variation of the resonant Raman cross section in the immediate neighborhood of the absorption threshold. The contribution of RRS to the attenuation coefficient is large in this region and it is important to establish whether the simple theory developed here is valid in other materials with different densities of states. If this turns out to be the case it may be a relatively straightforward matter to compile RRS correction to tabulated attenuation coefficients. It is expected that high-resolution studies of the spectral distribution currently being planned will yield much more information about the resonant Raman scattering process.

ACKNOWLEDGMENTS

We are grateful to the authorities at Laboratorie pour l'Utilization du Rayonnement Electromagnetique (LURE) for the provision of beam time on the DCI storage ring. The work was supported by research grants from the United Kingdom Science and Engineering Research Council (S.M. and M.J.C.) and the Finnish Academy of Sciences (S.M. and P.S.). We also wish to thank Dr. Chevalier for the loan of the silicon detector and the Laboratorie de Minéralogie-Cristallographie is "Unité No. 09 associée au Centre National de la Recherche Scientifique."

*Also at Laboratoire pour l'Utilisation du Rayonnement Electromagnétique (LURE), Université de Paris—Sud (Paris XI), Bâtiment 20929, 91405 Orsay Cédex, France.

[1]C. J. Sparks, Phys. Rev. Lett. **33**, 262 (1974).

[2]See for example, R. W. James, *The Optical Principles of the Diffraction of X-rays* (Bell, London, 1962).

[3]M. Gavrila and M. N. Tugulea, Rev. Roum. Phys. **20**, 209 (1975).

[4]T. Åberg and J. Tulkki, in *Atomic Inner-Shell Physics,* edited by B. Crasemann (Plenum, New York, 1985), Chap. 10.

[5]P. Suortti, Phys. Status Solidi B **91**, 657 (1979).

[6]J. Tulkki and T. Åberg, J. Phys. B **13**, 3341 (1980).

[7]H. Czerwinski, F. Smend, D. Schaupp, M. Schumacher, A. M. Millhouse, and H. Schenk-Strauss, Z. Phys. A **322**, 183 (1985).

[8]P. Eisenberger, P. M. Platzman, and H. Winick, Phys. Rev. B **13**, 2377 (1976).

[9]Y. B. Bannettt, D. C. Rapaport, and I. Freund, Phys. Rev. A **16**, 2011 (1977).

[10]S. Manninen, N. G. Alexandropoulos, and M. J. Copper, Philos. Mag. B **52**, 899 (1975).

[11]D. Schaupp, H. Czerwinski, F. Smend, R. Wenskus, M. Schumacher, A. M. Millhouse, and H. Schenk-Strauss, Z. Phys. A **319**, 1 (1984).

[12]F. Szmulowicz and D. M. Pease, Phys. Rev. B **17**, 3341 (1978).

[13]P. Suortti and L. D. Jennings, Acta Cryst. A **33**, 1012 (1977).

[14]D. C. Walters and C. P. Bhalla, Phys. Rev. A **3**, 1919 (1971).

[15]J. H. Hubbell, W. H. McMaster, N. Kerr Del Grande, and J. H. Mallett, in *International Tables for X-ray Crystallography* (Kynoch Press, Birmingham, 1974), Vol. IV.